Published in final edited form as:
Opt Express. 2008 May 12; 16(10): 7224–7232.

Three-dimensional *in vivo* imaging by a handheld dual-axes confocal microscope

Hyejun Ra[1,*], **Wibool Piyawattanametha**[1,2,3], **Michael J. Mandella**[1], **Pei-Lin Hsiung**[3], **Jonathan Hardy**[3], **Thomas D. Wang**[4], **Christopher H. Contag**[3], **Gordon S. Kino**[1], and **Olav Solgaard**[1]

[1]*Department of Electrical Engineering, Stanford University, Stanford, CA 94305, USA* [2]*NANOTEC/NECTEC, Pathumthani 12120, Thailand* [3]*James H. Clark Center for Biomedical Engineering and Sciences, and Department of Pediatrics, Radiology, and Microbiology & Immunology, Stanford University, Stanford, CA 94305, USA* [4]*Department of Internal Medicine, University of Michigan, Ann Arbor, MI 48109, USA*

Abstract

We present a handheld dual-axes confocal microscope that is based on a two-dimensional microelectromechanical systems (MEMS) scanner. It performs reflectance and fluorescence imaging at 488 nm wavelength, with three-dimensional imaging capability. The fully packaged microscope has a diameter of 10 mm and acquires images at 4 Hz frame rate with a maximum field of view of 400 μm × 260 μm. The transverse and axial resolutions of the handheld probe are 1.7 μm and 5.8 μm, respectively. Capability to perform real time small animal imaging is demonstrated *in vivo* in transgenic mice.

1. Introduction

There is an urgent need for *in vivo* imaging at cellular and subcellular resolution both for clinical applications and for small animal research. Medical diagnoses are typically based on histopathology after removal of tissues, which negates the possibility of real time information and limits the amount of tissue that can be analyzed. Small animal models are increasingly recognized as powerful discovery tools for mammalian biology, elucidating disease mechanisms and advancing therapies, especially with recent innovations in molecular probe designs and fluorescent markers. Interrogating biological changes at cellular resolution has typically required tissue acquisition via biopsy, or at the time of necropsy or autopsy. This constrains researchers to examining tissues out of context, or postmortem samples preventing longitudinal studies. The ability to examine *in vivo* pathologic conditions over time within living tissue, will refine diagnostic tools and stimulate the emerging field of *in vivo* pathology, enabling the full potential of small animal (intravital) imaging to be realized.

Confocal microscopy is a powerful imaging technique for this task, due to its capability to perform high resolution imaging and optical sectioning in both reflectance and fluorescence modes [1]. Reflectance imaging yields information on cell and tissue microanatomy. Fluorescence imaging enables the study of cell function through the use of targeted fluorescent

*Corresponding author: hra@stanford.edu

OCIS codes: (170.1790) Confocal microscopy; (170.2520) Fluorescence microscopy; (170.5810) Scanning microscopy; (170.6900) Three-dimensional microscopy.

probes and intravital dyes. Despite these advantages, *in vivo* application of confocal microscopy has been constrained by bulk optics. Significant effort has thus been put into miniaturization. Microelectromechanical systems (MEMS) devices offer innovative solutions to miniaturization [2-6]. However, conventional single-axis confocal microscopes have a tradeoff between resolution, size, and working distance (WD). The need for high resolution requires a larger high numerical aperture (NA) objective, resulting in a shorter WD. This presents a challenge in miniaturization, especially for applications requiring *in vivo* imaging at deep depths within tissue.

The dual-axes confocal architecture has been developed to overcome these limitations [7]. The design uses two low NA beams (illumination and collection) with overlapping focal volumes, amenable for miniaturization. This configuration offers several advantages. First, subcellular resolution is achieved in both transverse and axial dimensions. This is because the axial resolution decreases linearly with 1/NA, as opposed to $1/NA^2$ for the single-axis architecture. Second, the long WD provided by low NA lenses allows post-objective scanning, enabling larger field of view (FOV). Third, improved rejection of multiply-scattered photons in the collection beam enhances detection sensitivity and dynamic range compared to the single-axis architecture. This has been shown in Monte Carlo simulations [8].

Integration of a two-dimensional (2-D) MEMS scanner with the dual-axes confocal architecture enables the microscope system to be containable in a miniature package while enhancing imaging performance. We have previously reported on the design and fabrication of the MEMS scanner, and its integration with a dual-axes imaging system in a breadboard setup [9]. The first prototypes of the miniaturized package was demonstrated with *en face* reflectance imaging at 1315 nm wavelength [10], and fluorescence imaging at 785 nm wavelength [11,12], both of which focus on clinical applications. In this paper, we present a fully packaged handheld dual-axes confocal microscope capable of three-dimensional (3-D) reflectance and fluorescence imaging at 488 nm wavelength [13] for intravital imaging. We demonstrate real-time, volumetric imaging of transgenic mice both *ex vivo* and *in vivo*.

2. Methods

2.1 Optical system

A diagram of the imaging system is shown in Fig. 1. An optically pumped semiconductor laser at 488 nm wavelength is used as the light source. The laser light is coupled into a single mode fiber (SMF, Fibercore Limited, SM450) which collimates the beam using a graded index (GRIN) collimator (GRINTECH GmbH) at the distal end. The collimated beam is focused by a parabolic mirror, reflects off the MEMS scanner, and continues through a hemispherical lens (HL) into the sample. Signal from overlapping focal volumes within the sample propagates through the other optical branch. The collected photon signal is amplified by a photomultiplier tube (PMT). As the MEMS mirror raster scans the sample, signal from each pixel is collected and displayed on the computer screen as an *en face* image using a frame grabber and image acquisition software. 3-D volume data is obtained by translating the MEMS scanner in the z (depth)-direction using a computer-controlled piezoelectric actuator (Physik Instrumente, P-783), which varies the WD. The stack of 2-D *en face* images can later be compiled into a 3-D image. Imaging can be performed in reflectance mode or in fluorescence mode by inserting a long-pass optical filter ($\lambda > 494$ nm) in the collection path for the latter case.

A schematic diagram of the 10 mm diameter imaging head is shown in Fig. 2(a) with a photograph of the MEMS scanner mounted on a printed circuit board (PCB) in the inset. Fig. 2(b) shows the fully assembled handheld probe mounted in an upright position. The probe assembly starts with mounting two fiber-pigtailed GRIN collimators in the two precision machined v-grooves within the housing. The fibers are designed for single-mode operation at

488 nm wavelength. Then a pair of Risley prisms is mounted in each v-groove in front of the collimators to adjust for the illumination and collection beams to be parallel. This will ensure that the foci of the two beams will coincide after being focused by the parabolic mirror. The MEMS scanner is separately mounted on a PCB, and wirebonded to the PCB bondpads that are connected to wires running through the middle of the housing. The backplane that holds the PCB is connected to a z-translation stage that is actuated by the closed-loop piezoelectric actuator. Finally, the image head is sealed with UV-curing glue to prevent leakage when imaging live specimen.

2.2 MEMS scanner

An SEM image of the MEMS scanner is shown in Fig. 3. The overall chip size of the scanner is 3.2 mm × 2.9 mm. The scanner is metallized with a 12-nm-thick layer of aluminum to increase reflectivity for higher photon efficiency. This is important for fluorescence imaging to compensate for our lower collection NA of 0.11. Aluminum metallization increases our reflectivity by a factor of two from 37% to 74% compared to bare single crystalline silicon. Since the imaging beam reflects off the MEMS scanner twice before collection, the effective increase in photon efficiency is a factor of four. The radius of curvature for the metallized mirror is 95.4 cm, and the average surface roughness is 6 nm.

The resonance frequency of the scanner is 760 Hz and 2.43 kHz for the outer and inner axes, respectively. For 2-D *en face* imaging, rotation around the outer axis (V1 and V2) is resonantly driven at 760 Hz with a sine wave at maximum 45V, while rotation around the inner axis (V3 and V4) is driven at 4 Hz with a sawtooth waveform at maximum 75V, in order to maximize FOV. The sawtooth waveform is smoothed at the transition edges to mitigate higher frequency ringing on the inner axis. The opposite-side drive waveforms (V1 and V2 for the outer axis, and V3 and V4 for the inner axis) are 180° out of phase to maximize the linear region of motion.

2.3 Control and acquisition system

The imaging system is controlled using LabVIEW™ software and three National Instruments™ boards (two of PCI-6711, one of PCI-6115). The frequency and amplitude of four actuation signals control the frame rate and FOV of the MEMS scanner. The step size and depth range of the piezoelectric actuator can be adjusted to optimize acquisition of 3-D datasets. The PMT gain can also be synchronously adjusted to compensate for decreasing signal levels at increasing depths. Automated frame averaging and display can be performed to reduce noise and improve image quality during imaging. 2-D *en face* images from the analog input channel signal are acquired and displayed in real time to enable continuous monitoring of the image sample. All images are saved in 12-bit format. 3-D volume data can be rendered by post-processing using Amira® software.

3. Results

3.1 Probe Characterization

The probe is characterized in the reflectance mode by imaging a highly reflective US Air Force (USAF) target. The transverse resolution of the probe is acquired by the knife-edge method [15]. The measured full-width-half-maximum (FWHM) resolutions of the inner and outer scan axes are 1.7 μm and 3.2 μm, respectively. Figure 4 shows group 7 of the USAF target, where the last element, having a linewidth of 2.2 μm, is clearly resolved. The image plane is slightly curved due to the MEMS mirror scanning over an arched plane. The axial resolution is measured by actuating the piezoelectric actuator with a sawtooth waveform and translating the focus through a reflective mirror. The FWHM axial resolution is measured to be 5.8 μm. The measured values are slightly larger than the theoretical resolutions of 1.6 μm and 1.8 μm for the transverse dimensions, and 4.0 μm for the axial dimension [7]. This is mainly due to the

decrease in effective NA from the clipping of the collimated beam by the outer-axis dimension of the MEMS scanner chip. In addition, alignment errors occurred from the shifting of Risley prisms while fixing with UV-curing glue.

3.2 Fluorescence Imaging

3.2.1 Ex vivo imaging—Tissue imaging was performed with the handheld dual-axes confocal probe. We first imaged excised tissue obtained from transgenic mice expressing green fluorescent protein (GFP; B5/EGFP "Nagy" mouse, Jackson Laboratory). This transgenic strain expresses enhanced GFP (EGFP) throughout many tissues, although the level of expression varies between different organs [14]. Handheld probe images were taken at 4 frames per second over a maximum FOV of 400 μm × 260 μm and displayed in 400 × 190 pixels. Figure 5(a) and (c) show *en face* images of freshly excised tissue of a GFP mouse. Figure 5(a) shows an acquired image of adipocytes (fat cells) from the hind leg region. After imaging, the tissue was fixed in 10% buffered formalin, cut into 5 μm sections, and processed with routine hematoxylin and eosin (H&E) staining. This procedure is widely used for tissue morphologic interpretation and medical diagnosis. A representative histologic image from the same tissue block taken using a commercial wide-field microscope is shown in Fig. 5(b), where similar adipocytes are observed. Figure 5(c) displays the dual-axes confocal image of the villi structure in the small intestine, corresponding to histology in Fig. 5 (d). Two villi are clearly visible, illustrating the highly fluorescent enterocyte layer forming the boundary of the villi and surrounding the core lamina propria. Each image is an average of 4 frames. There is a good correspondence in structure and size between the acquired image and histology from the same tissue.

The 3-D imaging capability of the miniaturized probe is demonstrated in Fig. 6. Figure 6(a) shows three *en face* planes extracted from a 3-D volume rendering of the upper hind leg of a GFP mouse. The images are acquired at 35 μm, 65 μm, and 100 μm below the surface. For each z-section slice, distinct muscle structure is clearly resolved. The gain is increased with depth to compensate for lower signal levels. The movie file shows the entire image stack acquired from the surface to 130 μm depth. Figure 6(b) shows one frame from the stack at 65 μm depth. The striation patterns of skeletal muscle can be observed. Figure 6(c) shows images from a 3-D tissue volume of the front brain. The three planes are at depths of 12 μm, 40 μm, and 72 μm below the surface. The movie file shows the entire image stack acquired from the surface to 80 μm depth. Vessel-like structures are clearly visible connected throughout the volume. Each frame is an average of 4 frames. Color mapping is used in post-processing to better display the 12-bit data. No other image processing is applied. A maximum intensity projection image obtained from the 3-D rendering is shown in Fig. 6(d), showing the network of connected structures throughout the volume. The ability to compile a high resolution 3-D volume from 2-D *en face* image stacks demonstrates the power of optical sectioning from the handheld probe.

3.2.2 In vivo imaging—*In vivo* imaging was performed on a mouse anesthetized with Avertin (250 μL). Fluorescein isothiocyanate-dextran (FITC-dextran, 2,000,000 average molecular weight, 100μL) was injected into the retro-orbital plexus prior to imaging. Imaging was performed by resting the mouse on a stage and placing its intact ear on the hemispherical lens window of the inverted microscope. Figure 7(a) shows a 3-D volume rendering of the image stack obtained by scanning from the surface to 90 μm deep into the tissue. The images were taken in 2 μm intervals in depth with the piezoelectric actuator. All frames were taken at 4 frames per second with averaging of 4 frames. The full 3-D volume was acquired in 45 seconds. The maximum intensity projected image of the stack is shown in Fig. 7(b). The vessels containing the FITC-dextran solution can be clearly delineated in the image. Since FITC-

dextran slowly leaks out of the vessels over time, faint fluorescence signals outside the vessels can also be observed.

4. Discussion

The reported handheld dual-axes confocal microscope was developed primarily for small animal (intravital) imaging. We have tested our microscope system by collecting real-time images and 3-D data from transgenic mice, to assess imaging performance under intravital imaging conditions. One of our current limitations is the relatively low sample illumination power of 1.3 mW. This is due to the free-space coupling loss from the 488 nm laser into the input SMF, and insertion loss of the optical components along the beam path. This can be improved by having a higher power fiber-coupled laser source and increasing the metallization layer thickness of the MEMS scanner for higher reflectivity. Another challenge is alignment of the microscope assembly. Accurately aligning the collimated illumination and collection beams ensures that the two foci overlap. Although the Risley prism pairs are used for fine tuning the alignment of this process, the last curing step of UV adhesive shifts the components and creates misalignment. Use of smaller angle Risley prisms and low shrinkage UV curing adhesive will secure proper alignment.

In our *in vivo* experiments, fluorescence signal was acquired down to 150 μm depth at 488 nm wavelength. This demonstrates the large dynamic range from the dual-axes confocal architecture enabling deep subsurface imaging in tissue, in accordance with previous optical simulation results [8]. Images are acquired at 12 bits per pixel to accommodate the large dynamic range.

Figure 5(a) and (c) are 8-bit grayscale images as they are displayed on the computer screen during real-time image acquisition. In Figures 6 and 7, the stored raw data is presented in a colormap which displays the full range of signal intensity for every pixel. Signal levels usually fall within the 11-bit range. Color mapping gives better visual information of acquired images. Therefore, it will be valuable to integrate this display option in the real-time acquisition program.

The main goal of the handheld dual-axes confocal microscope is to perform high resolution 3-D *in vivo* intravital imaging in flexible positions and configurations. The microscope can be used for screening in handheld mode, then fixed in position at various angles and orientations for stable 3-D imaging.

5. Conclusion

We have demonstrated a handheld dual-axes confocal microscope operating at 488 nm wavelength for intravital imaging. The microscope is fully packaged and sealed, encasing a MEMS scanner that performs real-time 2-D *en face* imaging. Intravital imaging results show that the microscope can perform 3-D reflectance and fluorescence imaging *in vivo*. This will enable the acquisition of morphological and functional data in live animal models. All system components can be mounted on a portable unit to enable imaging in a variety of research settings.

Supplementary Material

Refer to Web version on PubMed Central for supplementary material.

Acknowledgements

The authors would like to thank Larry K. Wong, Jonathan T. C. Liu, and Robert P. J. Barretto for their technical assistance. This work was supported by the National Institutes of Health (grants U54 CA105296 and R33 CA109988). Pei-Lin Hsiung is supported by the Canary Foundation/American Cancer Society Early Detection Postdoctoral Fellowship.

References and links

1. Pawley, J., editor. Handbook of Biological Confocal Microscopy. Vol. 3rd ed.. Plenum; New York: 1996.
2. Dickensheets DL, Kino GS. Silicon-micromachined scanning confocal microscope. J. Microelectromech. Syst 1998;7:38–47.
3. Piyawattanametha, W.; Toshiyoshi, H.; LaCosse, J.; Wu, MC. Surface-micromachined confocal scanning optical microscope; Conference on Lasers and Electro-Optics, Technical Digest; Optical Society of America. 2000; p. 447-448.
4. Murakami, K.; Murata, A.; Suga, T.; Kitagawa, H.; Kamiya, Y.; Kubo, M.; Matsumoto, K.; Miyajima, H.; Katashiro, M. Technical Digest of Transducers. Boston: 2003. A miniature confocal optical microscope with MEMS gimbal scanner; p. 587-590.
5. Kwon S, Lee LP. Micromachined transmissive scanning confocal microscope. Opt. Lett 2004;29:706–708. [PubMed: 15072365]
6. Shin H-J, Pierce MC, Lee D, Ra H, Solgaard O, Richards-Kortum R. Fiber-optic confocal microscope using a MEMS scanner and miniature objective lens. Opt. Express 2007;15:9113–9122.http://www.opticsinfobase.org/abstract.cfm?URI=oe-15-15-9113
7. Wang TD, Mandella MJ, Contag CH, Kino GS. Dual-axis confocal microscope for high-resolution *in vivo* imaging. Opt. Lett 2003;28:414–416. [PubMed: 12659264]
8. Wong LK, Mandella MJ, Kino GS, Wang TD. Improved rejection of multiply scattered photons in confocal microscopy using dual-axes architecture. Opt. Lett 2007;32:1674–1676. [PubMed: 17572743]
9. Ra H, Piyawattanametha W, Taguchi Y, Lee D, Mandella MJ, Solgaard O. Two-Dimensional MEMS Scanner for Dual-Axes Confocal Microscopy. J. Microelectromech. Syst 2007;16:969–976.
10. Piyawattanametha, W.; Liu, JTC.; Mandella, MJ.; Ra, H.; Wong, LK.; Hsiung, P.; Wang, TD.; Kino, GS.; Solgaard, O. MEMS Based Dual-axes Confocal Reflectance Handheld Microscope for *in vivo* Imaging; Proceedings of IEEE International Conference on Optical MicroElectroMechanical Systems; Institute of Electrical and Electronics Engineers, Montana. August, 2006; p. 164-165.
11. Liu JTC, Mandella MJ, Ra H, Wong LK, Solgaard O, Kino GS, Piyawattanametha W, Contag CH, Wang TD. Miniature near-infrared dual-axes confocal microscope utilizing a two-dimensional microelectromechanical systems scanner. Opt. Lett 2007;32:256–258. [PubMed: 17215937]
12. Piyawattanametha, W.; Ra, H.; Mandella, MJ.; Liu, JTC.; Wong, LK.; Du, CB.; Wang, TD.; Contag, CH.; Kino, GS.; Solgaard, O. Three-dimensional *in vivo* Real Time Imaging by a Miniature Dual-axes Confocal Microscope based on a Two-dimensional MEMS Scanner; Proceedings of International Conference on Solid-State Sensors, Actuators, and Microsystems; Lyon, France. June, 2007; p. 439-442.
13. Ra, H.; Piyawattanametha, W.; Mandella, MJ.; Liu, JTC.; Wong, LK.; Wang, TD.; Contag, CH.; Kino, GS.; Solgaard, O. Three-Dimensional *in vivo* Reflectance and Fluorescence Imaging by a Handheld Dual-Axes Confocal Microscope; Conference on Lasers and Electro-Optics/Quantum Electronics and Laser Science and Photonic Applications Systems Technologies, Technical Digest (CD); Optical Society of America. May, 2007; paper CTuEE1. http://www.opticsinfobase.org/abstract.cfm?URI=CLEO-2007-CTuEE1
14. Hadjantonakis A-K, Gertsenstein M, Ikawa M, Okabe M, Nagy A. Generating green fluorescent mice by germline transmission of green fluorescent ES cells. Mech. Dev 1998;76:79–90. [PubMed: 9867352]
15. Siegman AE, Sasnett MW, Johnston TF Jr. Choice of clip levels for beam width measurements using knife-edge techniques. IEEE J. Quantum Electron 1991;27:1098–1104.

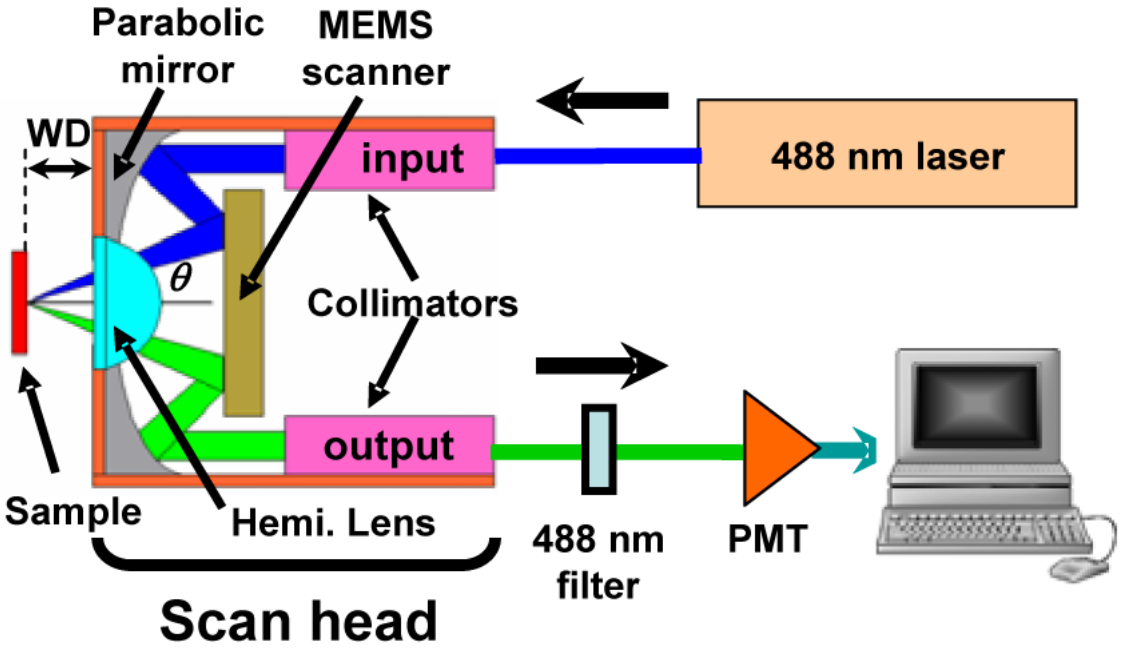

Fig. 1.
Diagram of the imaging system.

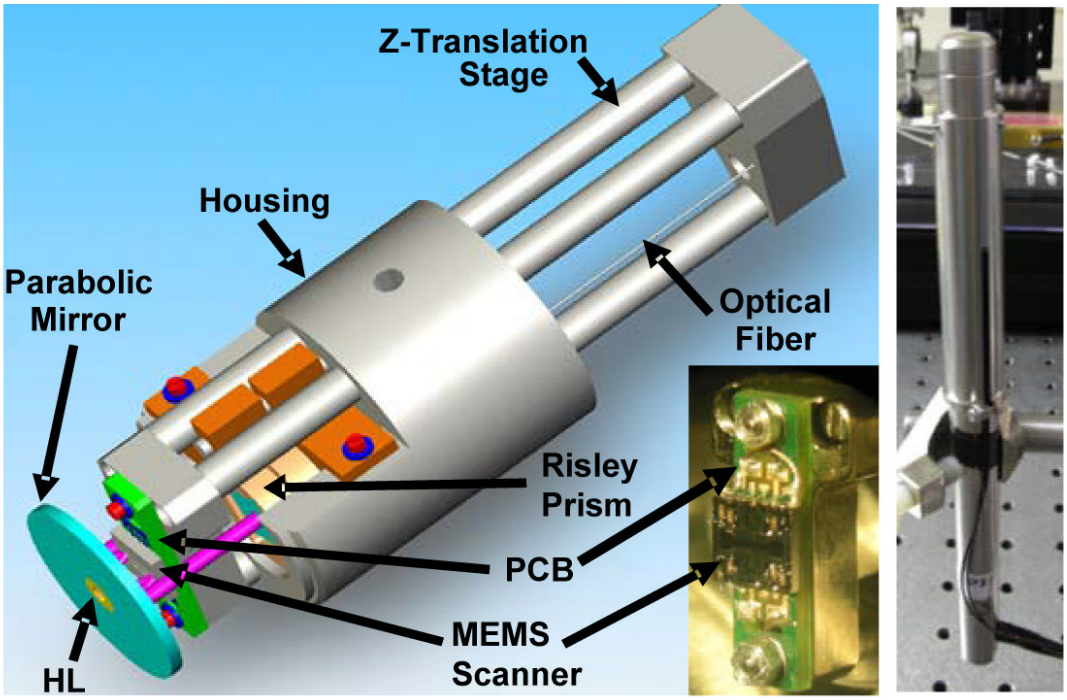

Fig. 2.
(a) Schematic of the 10 mm diameter handheld probe with the packaged MEMS scanner in the inset. (b) Photograph of the fully assembled dual-axes confocal handheld probe.

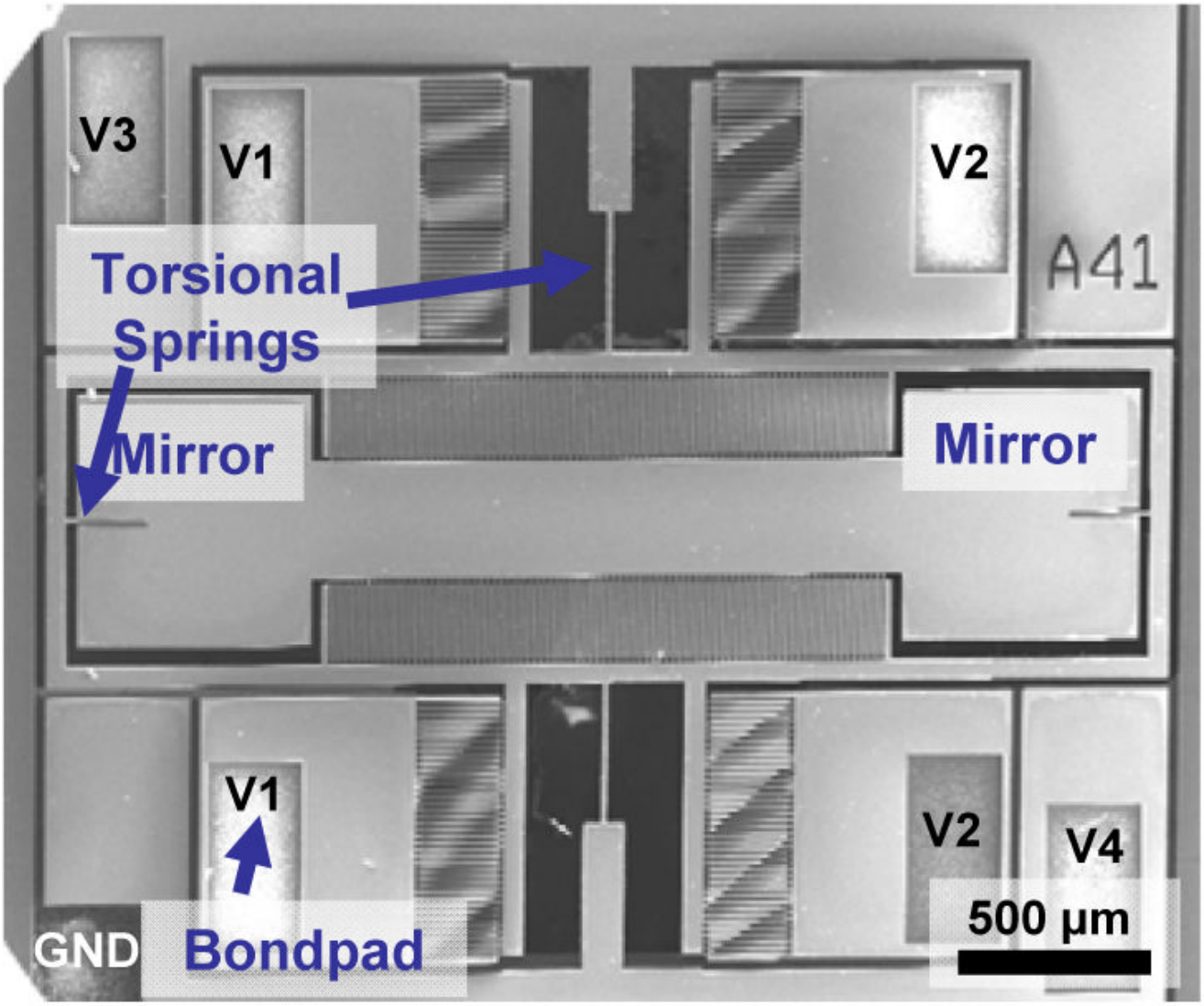

Fig. 3.
SEM of the MEMS scanner.

Fig. 4.
Reflectance image of group 7 of USAF target. Scale bar is 20 μm.

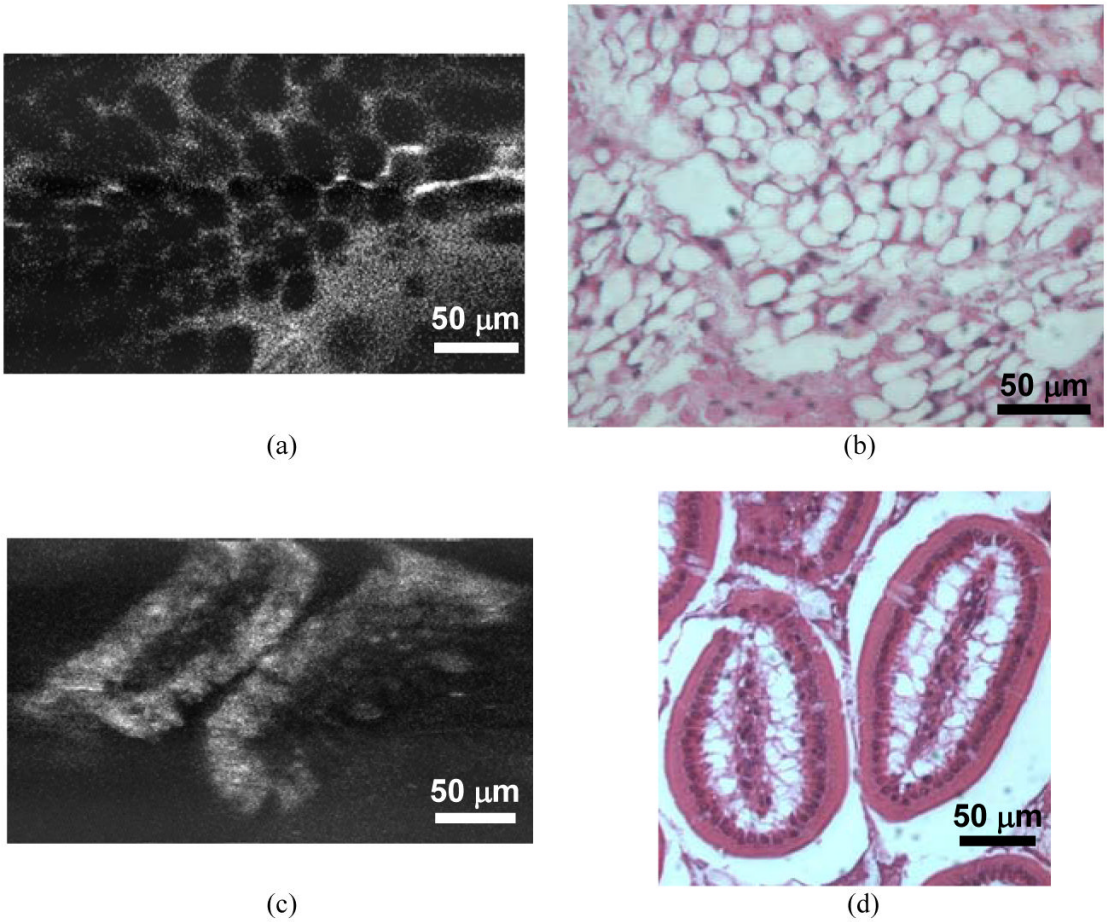

Fig. 5.

Ex vivo images of freshly excised GFP mouse tissue and corresponding histology. (a) Adipocytes in the hind leg region. (b) Histology of adipocytes. (c) Villi in the small intestine. (d) Histology of small intestine.

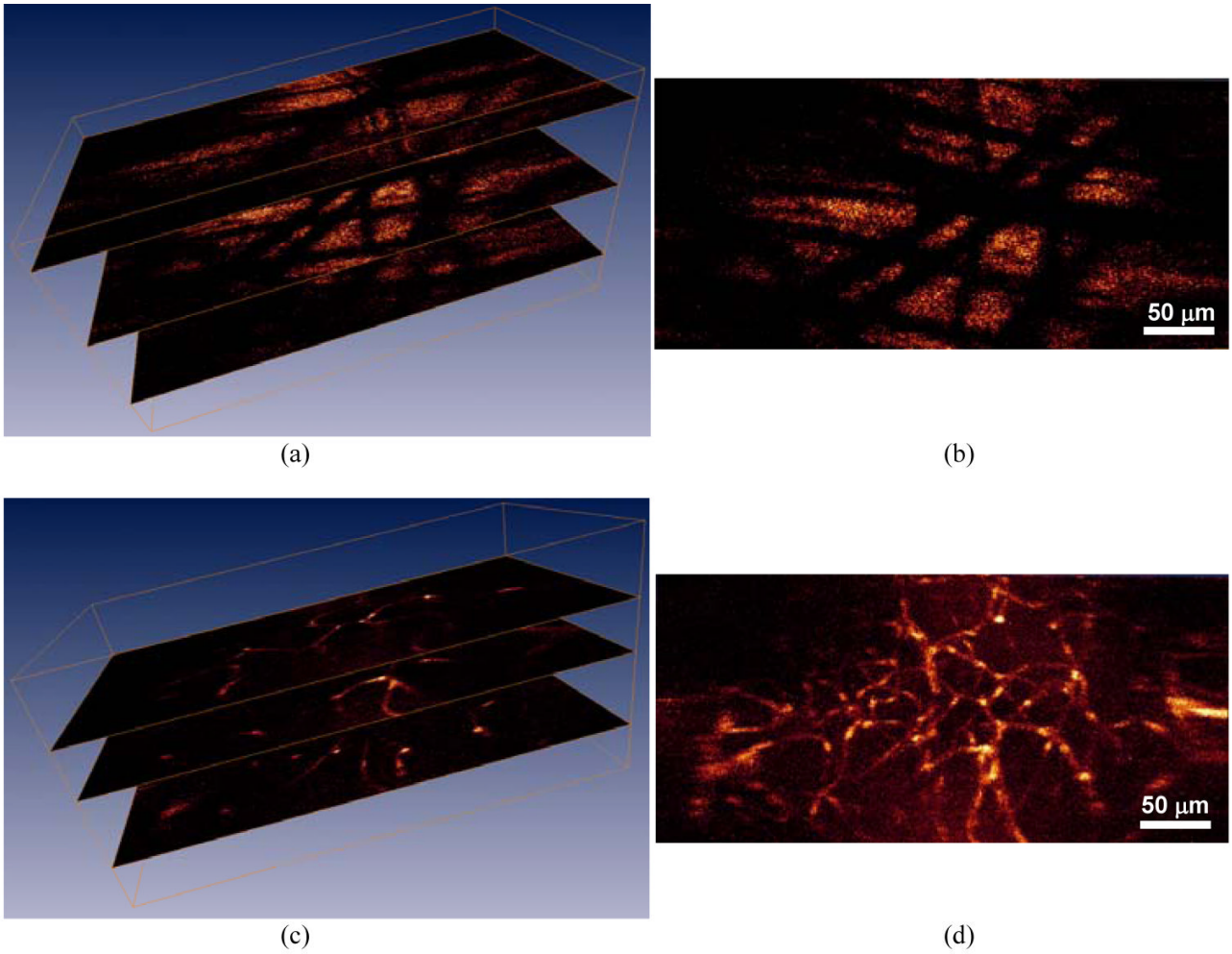

Fig. 6.

Ex vivo images of freshly excised GFP mouse tissue. Three *en face* planes extracted from a 3-D volume rendering and movies of the entire image stack are shown in (a) and (c). (a) Muscle. (Movie size 2.9 MB) (b) One *en face* image within the stack. (c) Vessel-like structures in the brain. (Movie size 2.7 MB) (d) Maximum intensity projected image of the stack.

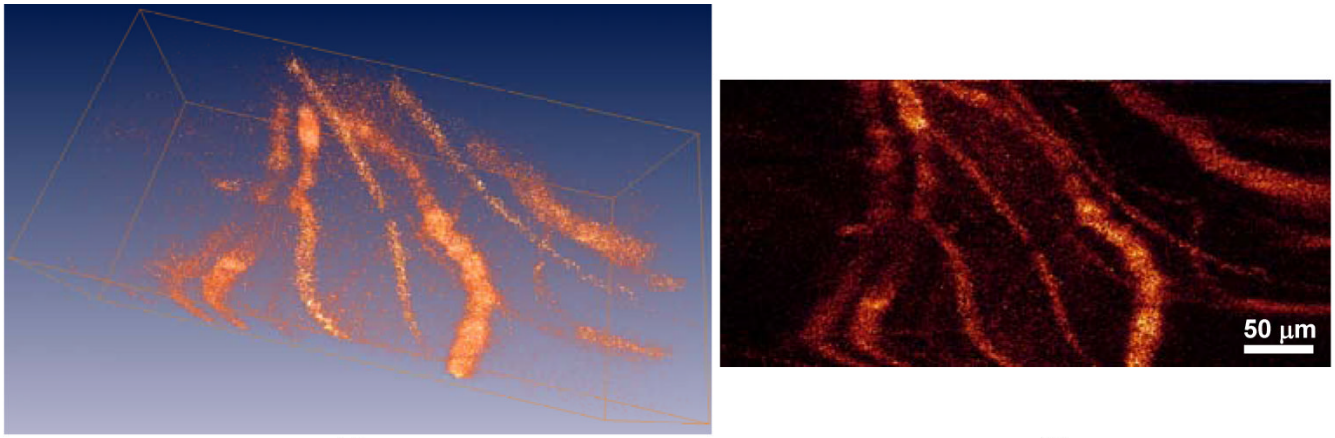

(a) (b)

Fig. 7.
In vivo image of blood vessels in an intact mouse ear. (a) 3-D volume rendering. (b) Maximum intensity projected image of the stack.